

Zr⁴⁺-Doped Anatase TiO₂ Nanotube Array Electrode for Electrocatalytic Reduction of L-cystine

Weizhen Wang, Guangxin Wang, Xuhui Zhao *, Xiaofeng Zhang, Yuming Tang * and Yu Zuo

Beijing Key Laboratory of Electrochemical Process and Technology for Materials, Beijing University of Chemical Technology, Beijing 100029, China;

Abstract: A Zr⁴⁺-doped anatase TiO₂ nanotube array electrode was prepared using a process that included Ti anodizing, chemical immersion, and heat treatment. The compositions, microstructure, and electrochemical properties of the prepared electrodes were characterized. The results show that Zr⁴⁺ was successfully introduced into the TiO₂ nanotube array electrodes. Because Zr⁴⁺ was doped into the crystal structure of the TiO₂ and replaced a part of Ti⁴⁺ to form more oxygen vacancies and Ti³⁺, the electrocatalytic activity of the prepared electrodes, for the reduction of L-cystine, was significantly improved.

Keywords: nanocomposites; oxidation; titanium dioxide; electrocatalysis

1. Introduction

L-cysteine is widely used in many fields, such as medicine, cosmetics, and biochemical research. The typical industrial production of L-cysteine is achieved through the electrocatalytic reduction of L-cystine. The currently used Pb electrodes, or other catalytic electrodes with deposited Pb, are prone to heavy metal pollution in acid electrolytes. Although titanium electrodes have also been used in the reduction of L-cystine, the effect is not satisfactory [1]. Therefore, developing alternative materials with stable performance, that are environmentally friendly and have a high catalytic reduction activity, are one of the current research hotspots [2–4].

As one of the most studied catalytic materials, TiO₂ has an important role in the field of catalysis [5–11]. Skúlason et al. [12] discussed the role of transition metal oxides in the electrocatalytic reduction of N₂ by using density functional theory (DFT) calculations. Hirakawa et al. [13] reported the role of oxygen vacancies and Ti³⁺ in TiO₂ in the photocatalytic reduction of N₂. In order to enhance the catalytic activity of TiO₂, doping metal elements are used to increase the vacancies and defects in the TiO₂ crystal structure [14–17]. At present, most of the correlative research in this field mainly focuses on the photocatalysis of TiO₂. However, there are relatively few studies on its electrocatalysis, especially regarding electrocatalytic reduction. Recently, Cao et al. [18,19] reported in detail that a Zr⁴⁺-doped TiO₂ electrode can efficiently reduce N₂ through electrocatalysis. This provides a feasible idea from which we can design a TiO₂ nanotube array electrode with a high electrocatalytic reduction activity for reducing L-cystine. Moreover, considering the better stability of titanium and the existence of the oxygen vacancies and Ti³⁺ in the anatase TiO₂, the TiO₂ nanotube array electrode might also possess good potential in the field of electrocatalytic reduction.

We have designed a Zr⁴⁺-doped anatase TiO₂ nanotube array electrode (anatase Zr/TiO₂), in which Zr⁴⁺ partly replaces Ti⁴⁺ in the anatase TiO₂, and studied its electrocatalytic reduction activity for reducing L-cystine and discussed its reduction mechanism.

We have designed a Zr⁴⁺-doped anatase TiO₂ nanotube array electrode (anatase Zr/TiO₂), in which Materials Zr⁴⁺ partly replaces Ti⁴⁺ in the anatase TiO₂, and studied its electrocatalytic reduction activity

2020, , 3572 2 2 of 7 for reducing L-cystine and discussed its reduction mechanism.

2. Materials and Methods

2. Materials and Methods

The preparation process for the anatase Zr/TiO₂ electrode is shown in Figure 1a. Firstly, the TiO₂ The preparation process for the anatase Zr/TiO₂ electrode is shown in Figure 1a. Firstly, the TiO₂

nanotube arrays on the pure Ti foil (99.99 wt%) surface was prepared through anodizing, which was carried out in 35 wt% (CH₂OH)₂ (ethylene glycol) + 0.5 wt% HF (hydrofluoric acid) solutions, under a carried out in 35 wt% (CH₂OH)₂ (ethylene glycol) + 0.5 wt% HF (hydrofluoric acid) solutions, under constant voltage of 20 V for 35 min at room temperature. The auxiliary electrode was a graphite a constant voltage of 20 V for 35 min at room temperature. The auxiliary electrode was a graphite

electrode. After anodization, the samples were soaked in deionized water and then chemically electrode. After anodization, the samples were soaked in deionized water and then chemically immersed in a 0.3 mol L⁻¹ Zr(NO₃)₄ solution for 4 h, in order to dope Zr⁴⁺. Subsequently, the samples immersed in a 0.3 mol·L⁻¹ Zr(NO₃)₄ solution for 4 h, in order to dope Zr⁴⁺. Subsequently, the samples were washed with deionized water and ethanol, several times. Finally, they were heated to 450 °C, were washed with deionized water and ethanol, several times. Finally, they were heated to 450 °C, kept for two hours, and cooled slowly in a mu e furnace. kept for two hours, and cooled slowly in a muffle furnace.

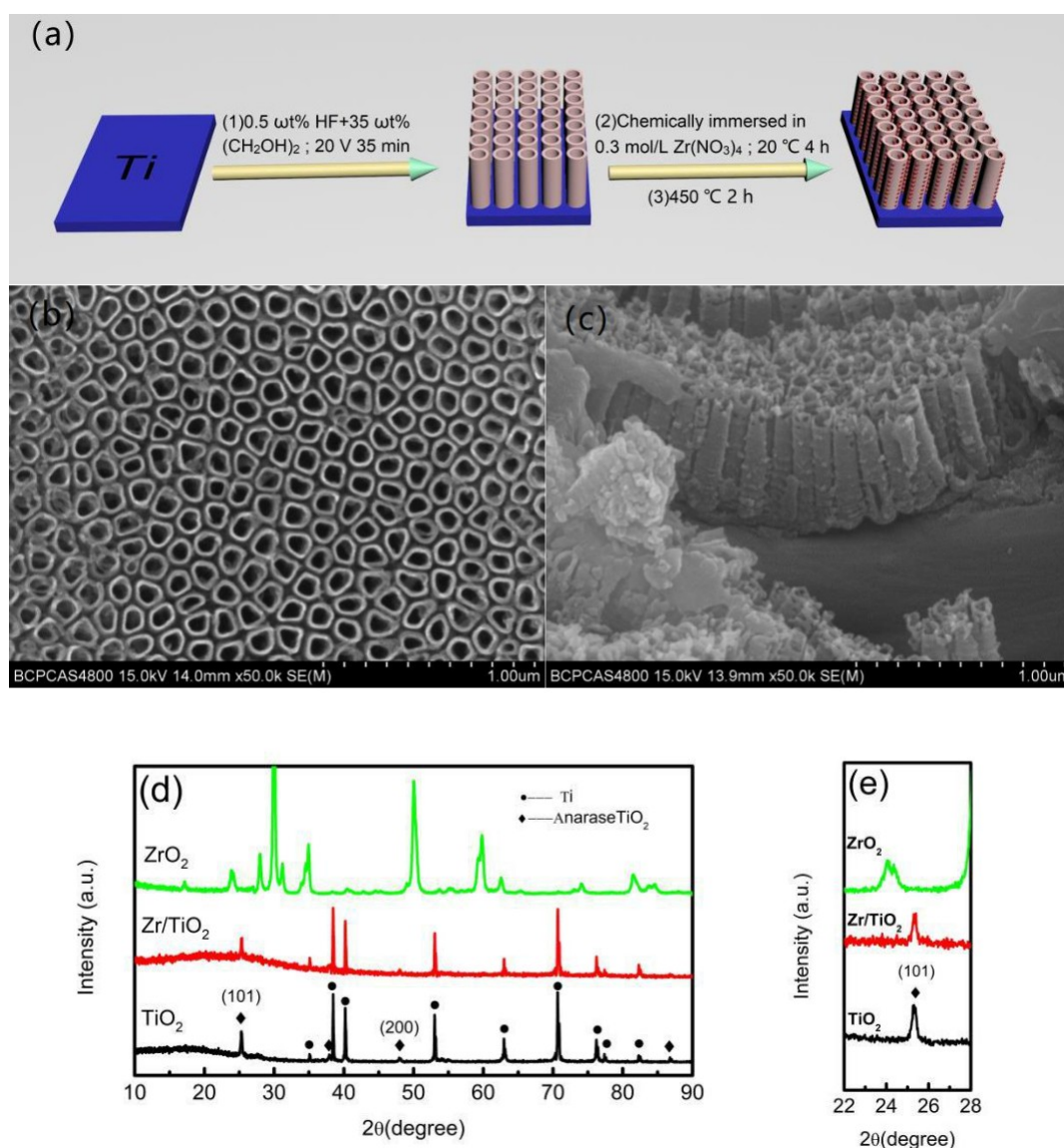


Figure 1. Preparation process (a), surface (b), and section (c) morphologies, and XRD patterns (d,e) of

Figure 1. Preparation process (a), surface (b), and section (c) morphologies, and XRD patterns (d,e) of anatase Zr/TiO₂ nanotube array electrode.

anatase Zr/TiO₂ nanotube array electrode.

The crystal structure of the modified electrode surface was studied using X-ray diffraction (XRD)

The crystal structure of the modified electrode surface was studied using X-ray diffraction (XRD) (Bruker D8 advance, Cu K α , λ = 0.1548 nm, Berlin, Germany). The morphology, length, and diameter

(Bruker D8 advance, Cu K α , λ = 0.1548 nm, Berlin, Germany). The morphology, length, and diameter of the TiO₂ nanotubes on the electrode surface were characterized using a SEM (S-4800, Hitachi,

Tokyo, Japan). The existence and valence of Ti and Zr on the surface of the Zr/TiO₂ electrode were characterized using X-ray photoelectron spectroscopy (XPS) (PHI 1600 ESCA, PerkinElmer, Waltham,

MA, USA). The binding energies of the peaks were calibrated using the binding energy of the C1s peak (285 eV).

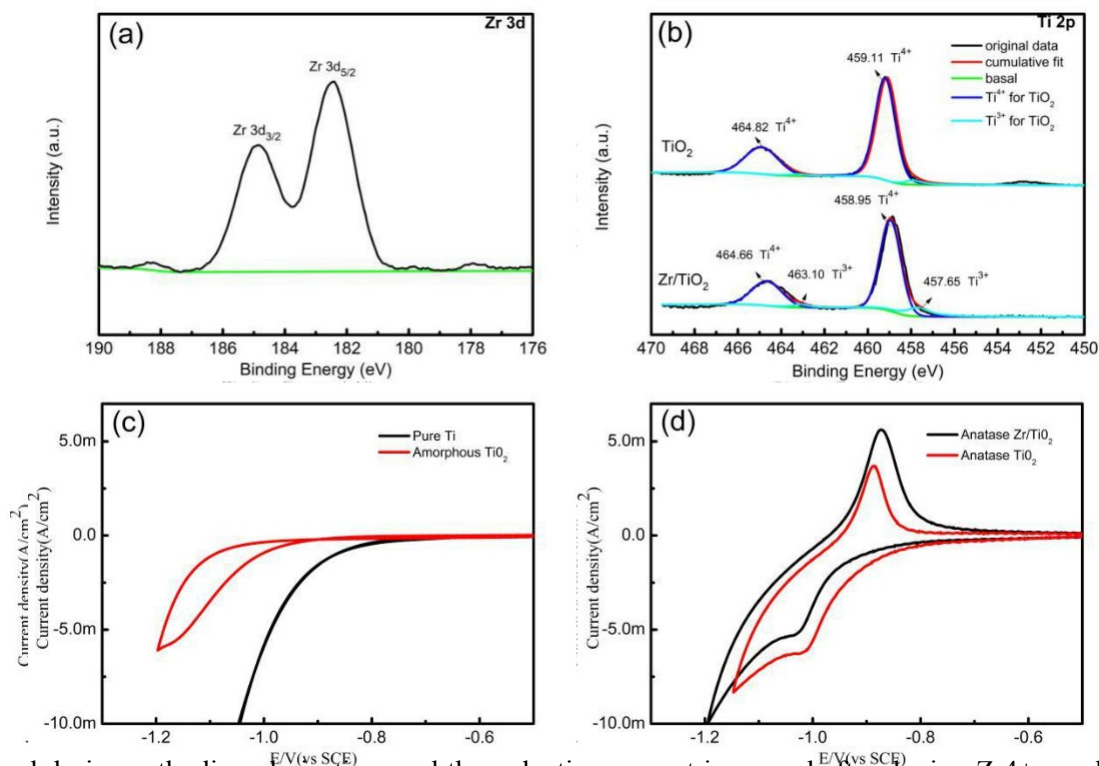
The electrochemical performance was tested using the electrochemical workstation (CS350H, Wuhan Corrtest, Wuhan, China). In the three-electrode system, the auxiliary electrode was a Pt electrode, and the reference electrode was a saturated calomel electrode. The test solutions were HCl solutions containing L-cystine.

3. Results

Scanning electron microscopy (SEM) images show that the anatase Zr/TiO₂ electrode has a tubular structure, with tube diameters and lengths of about 100 and 650 nm, respectively (Figure 1b,c). The crystalline structures of the different samples were studied using X-ray diffraction (Figure 1d)—for both the undoped and Zr⁴⁺-doped TiO₂ nanotube arrays. The other diffraction peaks correspond to the anatase phase (JCPDS # 21-1272). A close examination of the pattern (Figure 1e), after doping Zr⁴⁺, revealed that the peak intensity of the TiO₂ slightly decreased. According to the Scherrer equation, the calculated grain sizes of the TiO₂ (101) were about 7 and 5.1 nm for the undoped and doped samples, respectively, suggesting that the grain sizes of the TiO₂ also became slightly smaller after doping Zr⁴⁺. Above, the results indicate that the crystallinity of the TiO₂ slightly decreased. No diffraction peak relating to the ZrO₂ was observed in the XRD pattern (JCPDS # 79-1768). Compared to Ti⁴⁺, Zr⁴⁺ is suitable in size, and is similar in d electron configuration and oxide structure (Zr⁴⁺ 72 pm, Ti⁴⁺ 52 pm) [15]. Zr⁴⁺ was doped into the anatase TiO₂ to replace a part of Ti⁴⁺, and did not change the anatase crystal structure [18].

X-ray photoelectron spectroscopy (XPS) was used to characterize the chemical composition of the electrode surface. Figure 2 shows an overview of the XPS spectra for the undoped and Zr⁴⁺-doped TiO₂ nanotube array electrodes. The Zr⁴⁺-doped electrode surface is mainly composed of Ti and O, containing a small amount of Zr (about 2.44 atom. %). The peak of C1s may be attributed to the contaminants on the sample surface. In addition, the binding energies of the peaks were calibrated by the binding energy of the C1s peaks (285 eV). The Zr 3D spectra (Figure 3a) show two obvious peaks, revealing that the Zr element was on the surface of the electrode. However, there was no diffraction peak of ZrO₂ in the XRD pattern (Figure 1d), and the peak intensity of the TiO₂ slightly decreased; its peak positions moved slightly to the right after the doping of Zr⁴⁺ (Figure 1e), indicating that the Zr should be incorporated into the TiO₂ crystal lattice [20,21]. Figure 3b shows the deconvoluted XPS spectrum for the Ti 2p region. From the XPS-peak-differentiating analysis, it was found that, regardless of Zr⁴⁺-doping or not, Ti³⁺ and Ti⁴⁺ exist in the TiO₂ electrodes. The four peaks correspond to the Ti³⁺ 2p_{3/2} (457.65 eV), Ti⁴⁺ 2p_{3/2} (458.95 eV), Ti³⁺ 2p_{1/2} (463.10 eV), and Ti⁴⁺ 2p_{1/2} (464.66 eV) [20]. However, for the undoped TiO₂ nanotube array electrode, the Ti³⁺ content is very small (about 4.9 atom% of the total Ti). For the Zr⁴⁺-doped electrode, there is a significant increase in the area of two Ti³⁺ sub-peaks in Figure 3b, indicating an increase in the Ti³⁺ content (about 14.1 atom% of the total Ti). Compared with Figure 3c,d, the onset potential of the amorphous TiO₂ nanotube array electrode for a hydrogen evolution reaction (HER) is significantly more negative than that of the pure titanium electrode, but no other redox peak was observed in the cyclic voltammeteries (CVs) for both electrodes. However, for the undoped and Zr⁴⁺-doped anatase TiO₂ nanotube array electrodes, there were nearly reversible redox peaks in the CVs, which corresponded to a transformation between Ti⁴⁺ and Ti³⁺ [22]. Moreover, after doping Zr⁴⁺, the oxidation peak current decreased, and reduction peak current increased, which indicated that it is beneficial to transform Ti⁴⁺ into Ti³⁺ on the anatase Zr/TiO₂ nanotube array electrode. This is consistent with the previous XPS results.

Figure 2. XPS spectra of TiO₂ nanotube array surface: (a) Zr⁴⁺ doped; (b) undoped.



found during cathodic polarization, and the reduction current increased after doping Zr⁴⁺, as shown in Figure 4c,d. This indicates that the anatase structure of TiO₂ is helpful in the formation of Ti³⁺, and in Figure 4c,d. This indicates that the anatase structure of TiO₂ is helpful in the formation of Ti³⁺, and

as shown in Figure 4c,d. This indicates that the anatase structure of TiO₂ is helpful in the formation of Ti³⁺, and the dopant of Zr⁴⁺ can accelerate the transformation of Ti⁴⁺ to Ti³⁺. Moreover, when adding

Materials **2020**, *13*, x FOR PEER REVIEW 5 of 7 L-cystine to HCl solutions, the reduction currents increase in the two anatase TiO₂ nanotube array electrodes, before hydrogen evolution is observed, which suggests that the anatase TiO₂ possesses the the dopant of Zr⁴⁺ can accelerate the transformation of Ti⁴⁺ to Ti³⁺. Moreover, when adding 2 L-cystine electrocatalytic to HCl solutions, activities the reduction to reduce currents L-cystine increase. Compared in the two with anatase the undoped TiO₂ nanotube electrode, array electrothereductions,

current on the Zr⁴⁺-doped electrode has a more obvious increase, and the maximum difference in before hydrogen evolution is observed, which suggest that the anatase TiO₂ possesses the

current electrocatalytic (1.38 mA cm⁻²) activities² is about to reduc 2.26 times L-cystine that of. Compared the undoped with electro the undoped (0.61 mA cm⁻²) the², reduction These results

current on the 4+ Zr⁴⁺-doped electrode has a more obvious increase, and the maximum difference in prove that the Zr -doped TiO₂ nanotube array electrode has good electrocatalytic reduction activity

current (1.38 mA cm⁻²) is about 2.26 times that of the undoped electrode (0.61 mA cm⁻²). These results for reducing L-cystine. In order to illustrate the effect of the Zr dopant content, the electrocatalytic

prove that the Zr⁴⁺-doped TiO₂ nanotube array electrode has good electrocatalytic reduction activity activity of the electrodes prepared in the different concentrations of Zr(NO₃)₄ solution during the

for reducing L- cystine. In order to illustrate the effect of the Zr dopant content, the electrocatalytic chemical immersion process was studied using LSV, as shown in Figure 4e. From Figure 4e, the higher

activity of the electrodes prepared in the different concentrations of Zr(NO₃)₄ solution during the

the concentrations of the Zr(NO₃)₄ solution, the higher the electrocatalytic reduction activity of the chemical immersion process was studied using LSV, as shown in Figure 4e. From Figure 4e, the

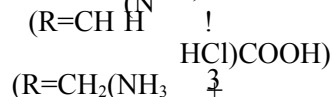
prepared electrode. This implies that the amount of Zr dopant increases with increasing concentrations higher the concentrations of the $Zr(NO_3)_4$ solution, the higher the electrocatalytic reduction activity of $Zr(NO_3)_4$ solution, from 0.15 to 0.30 mol L⁻¹. However, compared to the 0.30 mol L⁻¹ $Zr(NO_3)_4$ prepared electrode. This implies that the amount of Zr dopant increases with increasing

1mol·L⁻¹ $Zr(NO_3)_4$ solution, activity from 0.15 to 0.30 mol·L⁻¹. However, prepared compared in the 0.45 to 0.30 mol·L⁻¹ $Zr(NO_3)_4$ solution, obviously the electrocatalytic improved. Figure 4f shows activity schematic of the electrode diagram prepared of the catalytic the 0.45 mol·L⁻¹ reduction.

$Zr(NO_3)_4$ solution was not obviously. Figure 4f shows a schematic diagram of the mechanism that reduces L-cystine on the Zr^{4+} -doped TiO_2 nanotube array electrode. Because Zr^{4+} has a similar d electron configuration and oxide structure to but larger ionic size than Ti^{4+} , doping Zr^{4+} could not alter the crystalline structure of the anatase TiO_2 , but it did create the stress therein [15].

Ti^{4+} , doping Zr^{4+} could not alter the crystalline structure of the anatase TiO_2 , but it did create the stress. The strained effect induced the formation and enrichment of the adjacent bi- Ti^{3+} , which also resulted in the increased oxygen vacancies. These are beneficial to the enhancement of active centers [15,16]. The Ti^{3+} ions have a stronger attraction to the S atom of L-cysteine, to induce the S=S bond to break down. Therefore, doping Zr^{4+} improves the electrocatalytic activity of the anatase TiO_2 nanotube array electrode for L-cystine reduction.

L-cystine is not compatible with water, but it is easily soluble in acidic solutions. The reaction equation for the dissolution of L-cystine is [1]:



The anatase TiO_2 has oxygen vacancies and Ti^{3+} under a negative potential polarization. The reaction equation is [1]:

The anatase TiO_2 has oxygen vacancies and Ti^{3+} under a negative potential polarization. The reaction equation is [1]: $TiO_2 + 4H^+ + e^- \rightarrow Ti^{3+} + 2H_2O$ (2)

Under the negative potential polarization, the Ti^{3+} reacts with the dissolved $RSSR \cdot HCl$ in solution, as follows:

Under the negative potential polarization, the Ti^{3+} reacts with the dissolved $RSSR \cdot HCl$ in the solution, as follows:



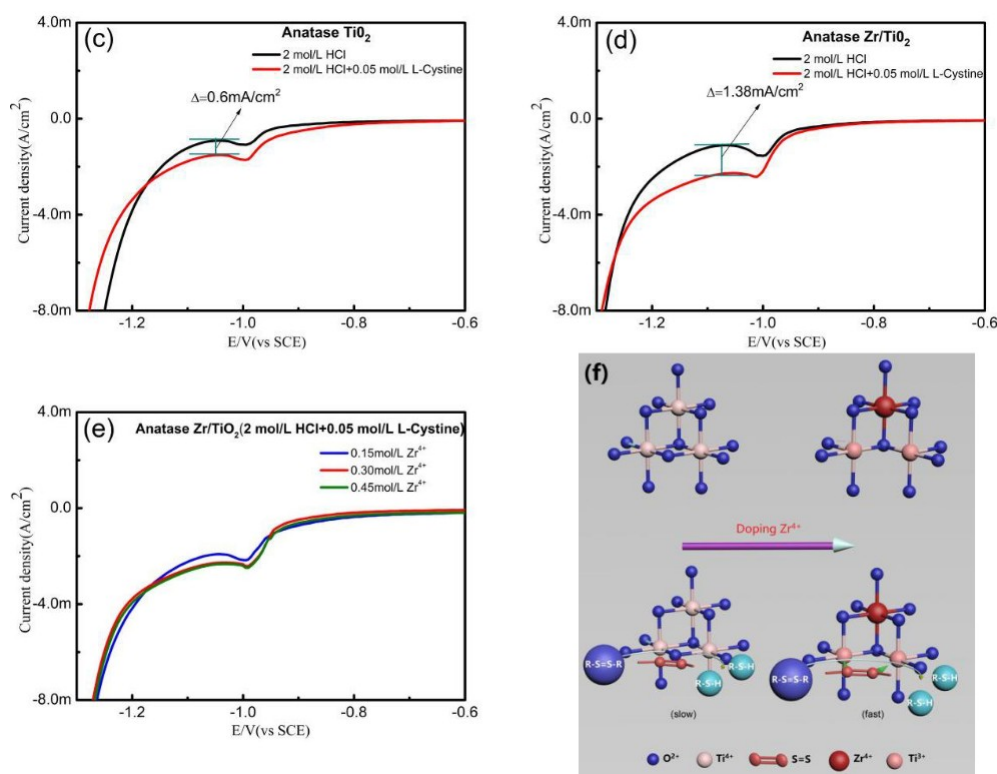


Figure 4. Linear sweep voltammetry (LSV) curves of different electrodes in 2 mol·L⁻¹ HCl or 2 mol·L⁻¹ HCl + 0.05 mol·L⁻¹ L-cystine solutions (scan rate: 5 mV·s⁻¹): (a) pure titanium, (b) amorphous TiO₂ nanoarray tube, (c) anatase TiO₂ nanoarray tube, and (d) anatase Zr/TiO₂ nanotube array electrode; nanoarray tube, (e) the influence of concentrations of Zr(NO₃)₄ solution in chemical immersion process; (f) schematic illustration of electrocatalytic reduction mechanism of the anatase Zr/TiO₂ nanotube array electrode for L-cystine.

Figure 4. Linear sweep voltammetry (LSV) curves of different electrodes in 2 mol·L⁻¹ HCl or 2 mol·L⁻¹ HCl + 0.05 mol·L⁻¹ L-cystine solutions (scan rate: 5 mV·s⁻¹): (a) pure titanium, (b) amorphous TiO₂ nanoarray tube, (c) anatase TiO₂ nanoarray tube, and (d) anatase Zr/TiO₂ nanotube array electrode; nanoarray tube, (e) the influence of concentrations of Zr(NO₃)₄ solution in chemical immersion process; (f) schematic illustration of electrocatalytic reduction mechanism of the anatase Zr/TiO₂ nanotube array electrode for L-cystine.

4. Conclusions

The Zr⁴⁺-doped anatase TiO₂ nanotube array electrode was prepared through anodizing, combined with chemical immersion and heat treatment. Zr⁴⁺-doping into the anatase TiO₂ induces the transformation of Ti⁴⁺ to Ti³⁺ and the formation of the oxygen vacancies, improving the electrocatalytic activity of the as-prepared electrode for L-cysteine reduction.

Author Contributions: Conceptualization, X.Z. (Xuhui Zhao) and Y.T.; methodology, W.W.; investigation, G.W.; writing—original draft preparation, W.W.; writing—review and editing, X.Z. (Xuhui Zhao) and Y.T.; **Author Contributions:** Conceptualization, X.Z. (Xuhui Zhao) and Y.T.; methodology, W.W.; investigation, G.W.; visualization, W.W. and G.W.; supervision, Y.Z. and X.Z. (Xiaofeng Zhang); funding acquisition, X.Z. (Xuhui Zhao)

writing—original draft preparation, W.W.; writing—review and editing, X.Z. (Xuhui Zhao), and Y.T.; visualization, Zhao). All authors have read and agreed to the published version of the manuscript.

W.W. and G.W.; supervision, Y.Z. and X.Z. (Xiaofeng Zhang); funding acquisition, X.Z. (Xuhui Zhao). All authors have read and agreed to the published version of the manuscript. This research was funded by the National Key Research and Development Program of China, grant number 2017YFB0307500.

Funding: This research was funded by the National Key Research and Development Program of China, grant number 2017YFB0307500.

Conflicts of Interest: The authors declare no conflict of interest.

Conflicts of Interest: The authors declare no conflict of interest.

References 1. Ralph, T.R.; Hitchman, M.L.; Millington, J.P.; Walsh, F.C. The reduction of L-cystine hydrochloride at stationary and rotating disc mercury electrodes. *Electrochim. Acta* **2005**, *51*, 133–145.

1. Ralph, T.R.; Hitchman, M.L.; Millington, J.P.; Walsh, F.C. The reduction of L-cystine hydrochloride at stationary and rotating disc mercury electrodes. *Electrochim. Acta* **2005**, *51*, 133–145. [\[CrossRef\]](#)
2. Yang, S.; Li, G.; Liu, L.; Wang, G.; Wang, D.; Qu, L. Preparation of nickel oxide nanoparticles on N-doped reduced graphene oxide: A two-dimensional hybrid for electrocatalytic sensing of L-cysteine. *J. Alloy. Comp.* **2017**, *691*, 834–840. [\[CrossRef\]](#)
3. Nosal-Wiercinska, A. The catalytic activity of cysteine and cystine on the electroreduction of Bi(III) ions. *J. Electroanal. Chem.* **2011**, *662*, 298–305. [\[CrossRef\]](#)
4. Wei, M.; Guo, J.; Shi, Z.; Yuan, Q.; Pu, M.; Rao, G.; Duan, X. Preparation and characterization of L-cystine and L-cysteine intercalated layered double hydroxides. *J. Mater. Sci.* **2007**, *42*, 2684–2689. [\[CrossRef\]](#)
5. Ke, D.; Liu, H.; Peng, T.; Liu, X.; Dai, K. Preparation and photocatalytic activity of WO₃/TiO₂ nanocomposite particles. *Mater. Lett.* **2008**, *62*, 447–450. [\[CrossRef\]](#)
6. Kment, S.; Riboni, F.; Pausova, S.; Wang, L.; Wang, L.Y.; Han, H.; Hubicka, Z.; Krysa, J.; Schmuki, P.; Zboril, R. Photoanodes based on TiO₂ and -Fe₂O₃ for solar water splitting—superior role of 1D nanoarchitectures and of combined heterostructures. *Chem. Soc. Rev.* **2017**, *46*, 3716–3769. [\[CrossRef\]](#)
7. Qin, P.; Paulose, M.; Ibrahim Dar, M.; Moehl, T.; Arora, N.; Gao, P.; Varghese, O.K.; Grätzel, M.; Nazeeruddin, M.K. Stable and efficient perovskite solar cells based on Titania nanotube arrays. *Small* **2015**, *11*, 5533–5539. [\[CrossRef\]](#)
8. Liang, X.P.; Lian, Z.W.; Zhu, J.; Men, K.; Wei, F. The preparation and properties of TiO₂ nano-porous layers for perovskite solar cells. *AIP Adv.* **2020**, *10*, 015058. [\[CrossRef\]](#)
9. Ozkan, S.; Ghanem, H.; Mohajernia, S.; Hejazi, S.; Fromm, T.; Borchardt, R.; Rosiwal, S.; Schmuki, P. Boron-doped diamond as an efficient back contact to thermally grown TiO₂ photoelectrodes. *ChemElectroChem* **2019**, *6*, 4545–4549. [\[CrossRef\]](#)
10. Zhang, Y.; Pan, C. TiO₂/graphene composite from thermal reaction of graphene oxide and its photocatalytic activity in visible light. *J. Mater. Sci.* **2011**, *46*, 2622–2626. [\[CrossRef\]](#)
11. Zhang, W.; Shironita, S.; Umeda, M. Low Pt loading and high hydrogen oxidation reaction performance at Pt/TiO₂–SiO₂ investigated by a porous microelectrode. *Catal. Lett.* **2014**, *144*, 112–116. [\[CrossRef\]](#)
12. Skúlason, E.; Bligaard, T.; Gudmundsdóttir, S.; Studt, F.; Rossmeisl, J.; Abild-Pedersen, F.; Vegge, T.; Jónsson, H.; Nørskov, J.K. A theoretical evaluation of possible transition metal electro-catalysts for N₂ reduction. *Phys. Chem. Chem. Phys.* **2012**, *14*, 1235–1245. [\[CrossRef\]](#) [\[PubMed\]](#)

13. Hirakawa, H.; Hashimoto, M.; Shiraishi, Y.; Hirai, T. Photocatalytic conversion of nitrogen to ammonia with water on surface oxygen vacancies of titanium dioxide. *J. Am. Chem. Soc.* **2017**, *139*, 10929–10936. [[CrossRef](#)] [[PubMed](#)]
14. Chen, X.B.; Liu, L.; Yu, P.Y.; Mao, S.S. Increasing solar absorption for photocatalysis with black hydrogenated titanium dioxide nanocrystals. *Science* **2011**, *331*, 746–750. [[CrossRef](#)] [[PubMed](#)]
15. Song, L.; Zhang, R.; Zang, S.; He, H.; Su, Y.; Qiu, W.; Sun, X. Activity of selective catalytic reduction of NO over V₂O₅/TiO₂ catalysts preferentially exposed anatase {001} and {101} facets. *Catal. Lett.* **2017**, *147*, 934–945. [[CrossRef](#)]
16. Krbal, M.; Sopha, H.; Pohl, D.; Benes, L.; Damm, C.; Rellinghaus, B.; Kupčik, J.; Bezdička, P.; Šubrt, J.; Macak, J.M. Self-organized TiO₂ nanotubes grown on Ti substrates with different crystallographic preferential orientations: Local structure of TiO₂ nanotubes vs. photo-electrochemical response. *Electrochim. Acta* **2018**, *264*, 393–399. [[CrossRef](#)]
17. Saputera, W.H.; Mul, G.; Hamdy, M.S. Ti³⁺-containing titania: Synthesis tactics and photocatalytic performance. *Catal. Today* **2015**, *246*, 60–66. [[CrossRef](#)]
18. Cao, N.; Chen, Z.; Zang, K.; Xu, J.; Zhong, J.; Luo, J.; Xu, X.; Zheng, G. Doping strain induced bi-Ti³⁺ pairs for efficient N₂ activation and electrocatalytic fixation. *Nat. Commun.* **2019**, *10*, 2877. [[CrossRef](#)]
19. Shi, M.M.; Bao, D.; Wulan, B.R.; Li, Y.H.; Zhang, Y.F.; Yan, J.M.; Jiang, Q. Au sub-nanoclusters on TiO₂ toward highly efficient and selective electrocatalyst for N₂ conversion to NH₃ at ambient conditions. *Adv. Mater.* **2017**, *29*, 1606550. [[CrossRef](#)]
20. Lucky, R.A.; Charpentier, P.A. N-doped ZrO₂/TiO₂ bimetallic materials synthesized in supercritical CO₂: Morphology and photocatalytic activity. *Appl. Catal. B Environ.* **2010**, *96*, 516–523. [[CrossRef](#)]
21. Reddy, M.V.; Sharma, N.; Adams, S.; Rao, R.P.; Peterson, V.K.; Chowdari, B.V.R. Evaluation of undoped and M-doped TiO₂, where M = Sn, Fe, Ni/Nb, Zr, V, and Mn, for lithium-ion battery applications prepared by the molten-salt method. *RSC Adv.* **2015**, *5*, 29535. [[CrossRef](#)]
22. Macak, J.M.; Gong, B.G.; Hueppe, M.; Schmuki, P. Filling of TiO₂ nanotubes by self-doping and electrodeposition. *Adv. Mater.* **2010**, *19*, 3027–3031. [[CrossRef](#)]